Molecular dynamics studies of entangled polymer chains

Bulacu, Monica Iulia

Chapter 6

Polymer–polymer adhesion via connector chains

A good scientist is one who knows enough to steal from the best people.

J. Holton

Coarse-grained molecular-dynamics simulations have been performed to study the adhesion between two glassy polymers reinforced with connector chains. By computing the total work needed to completely separate the polymer bulks by pulling out the connector chains, we investigate the effects on the adhesion strength of different connector architectures (areal density, chain length and stiffness, number of stitches at the interface) and external debonding conditions (separation rate and temperature). The dependences of the adhesion strength G on connector length as n^2, on areal density as Σ^1, and on pulling velocity as v_{pull}^{α} (with α dependent on temperature) have been recovered for different number of stitches and for different connector rigidities. The time evolutions of the adhesion work from debonding simulations performed at various temperatures and pulling velocities collapse on a master curve when plotted in normalized units. An interesting observation concerns the number of stitches at the interface: the total work of adhesion is not markedly influenced by increasing the numbers of stitches. We find that chain stiffness also induces only a moderate increase in adhesion strength.

[0]Based on *Tensile debonding simulations of polymer-polymer interface reinforced with connector chains*, Monica Bulacu and Erik Van der Giessen, submitted to Macromolecules (2007).

6.1 Introduction

Bonding together existing polymers is a technical solution for creating new materials with specific properties, at a relatively low cost. For industrial applications, however, the overwhelming majority of polymers that require to be bonded are immiscible, thus having a very weak interfacial interaction. One strategy to increase the adhesion between such polymers is to improve the natural chain entanglement at the interface by adding supplementary connecting molecules at the interface (Creton et al. 2001). These preformed connectors link the polymer bulks and they effectively "sew" the junction and strengthen the interface adhesion often more than a hundred times, depending on their architecture. The adhesive bonding obtained is required to resist to different stress conditions and loading rates depending on the specific application and working environment: a very high adhesion strength is required in the construction and automotive industry, while a relatively low one is needed for the packaging industry.

The reinforcement produced by the connectors placed at the interface depends on their areal density, molecular weight and chain stiffness, as well as their spatial conformation, essentially, the way in which they weave back and forth across the interface to create one or multiple stitches (see Fig. 6.1).

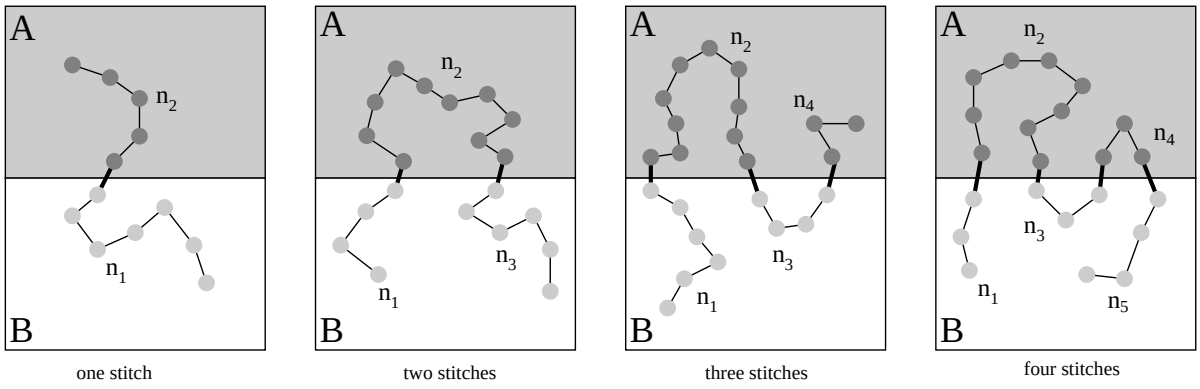

Figure 6.1: *Schematic representation of the stitch architecture of connectors at the interface between two glassy polymer bulks A and B. The number of stitches in the figure varies from $s = 1$ up to $s = 4$. The stitches are represented as thick bonds and the connector length is the sum of connector blocks $n = \sum_{i=1}^{s+1} n_i$. Each successive connector block is immersed in a different polymer bulk.*

A long and costly trial-and-error process is needed in applications in order to chose the specific connector architecture that leads to the intended adhesion strength for solving particular problems. The effects of the connector chains on the toughness of the interface between two immiscible glassy polymers have been extensively investigated.

The most common examples involve poly(methyl methacrylate)–PMMA, polystyrene–PS and polyvinylpyridine–PVP (e.g. Brown et al. 1993, Kramer et al. 1994, Washiyama et al. 1993, Dai et al. 1997).

An attractive alternative for selecting the adequate connector chains is to use computer programs to simulate various possibilities and extract guidelines for synthesizing specific polymers for the required mechanical response and interface strength. However, such achievement is not straightforward due to the complexity of the adhesion process, whose understanding involves multiple approaches coming from chemistry, interfacial physics, and mechanics.

The only available method for the quantitative evaluation of adhesion strength is the effective breakage of the interface. This justifies the traditional macroscopic approach of studying adhesion using fracture mechanics. But the measured fracture energy is many orders of magnitude greater than the theoretical sum of the free energies of the two newly created surfaces (following Griffith 1920). The generally accepted explanation for this difference is that the polymer–polymer fracture is not a reversible process, but rather consists of many irreversible dissipation processes, such as shear yielding or craze. Furthermore, subsequent detailed investigation of the fracture surfaces, using ion-beam and X-ray scattering techniques (Kramer 1991, Boucher et al. 1996), reveals that irregular material discontinuities appear at the crack tip, so that the true surface area becomes greater than the planar geometrical area assumed in classical fracture mechanics. For the case of polymer-polymer interface reinforced with connector chains, especially, the stress transfer is done by the connector chains and the adhesion strength is directly related to the entanglement of the connectors with the bulk chains.

Despite the importance of the molecular processes in adhesion strength, until the present, the analysis of polymer fracture has mostly concentrated on macroscopic phenomena. Nevertheless, some attempts have been made to incorporate the molecular fracture mechanisms into continuum models by using cohesive laws – phenomenological relations – between the traction on the interface and separation of the materials on either side. But, due to the lack of development of such laws for polymeric materials, these constitutive relations were just borrowed from those developed for metals, in spite of the clear distinction between the phenomenology of plastic deformation in amorphous polymers compared to metals. For example, Rahul-Kumar et al. (1999, 2000), modeling fracture during the peel test of viscoelastic polymers, showed the inadequacy of the metallic cohesive law. The major insufficiency is that the cohesive laws for polymers have to incorporate rate dependence.

One important aim of the study reported in this chapter is to develop constitutive relations specific for the debonding of a polymer–polymer interface reinforced with connector chains. This is achieved by performing molecular-dynamics simulations of the polymeric material localized in front of the crack tip (see Fig. 6.2). The novel constitutive

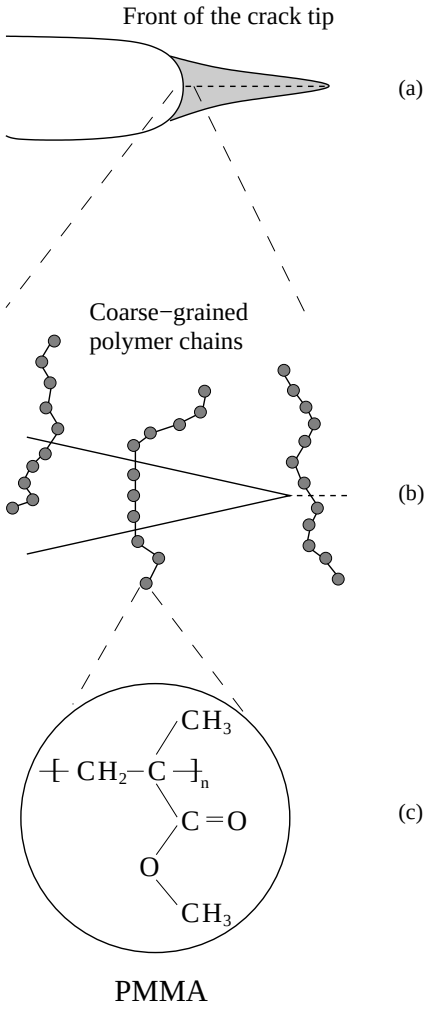

Figure 6.2: *The representation of the polymer fracture model: (a) the small scale plastic zone in the proximity of the crack tip where the molecular fracture mechanisms occur (e.g. pullout of the connector chains); (b) the mesoscopic molecular scale where the molecular dynamics simulations of the debonding are performed. The polymer chains are treated as strings of beads connected by springs; (c) the polymer bead – more polymer units collapsed together (e.g. for poly(methyl methacrylate) PMMA).*

relations can be used as cohesive laws at the continuum level in a multi-scale simulation. Such an implementation has been already done for simulating crack growth in homopolymers: using a micromechanical model, a cohesive law for crazing was derived and subsequently introduced in continuum fracture simulations (Tijssens et al. 2000, Tijssens and Van der Giessen 2000).

The major contribution of the traction-separation laws resulting from molecular dynamics is that they contain naturally the rate-dependent behavior of the system.

Besides this, we are particularly interested in the effects on the adhesion strength of the length of the connector chains, areal density, pulling velocity and temperature. The novelty of this work consists in the investigation of these effects together with the control of the stiffness along the connector backbone. We will also control the number of stitches that connectors form at the interface. The results presented here are the first MD study that explicitly and systematically considers the case of multiple stitches in between two polymer bulks modeled as realistic 3D ensembles of interacting polymer chains. Some previous attempts contain either end-grafted chains in a 3D bulk (Sides et al. 2001, Sides et al. 2002, Sides et al. 2004) or one multiple-stitch connector in between two networks of obstacles in 2D (Pickett et al. 1996, Pickett et al. 1997, Sabouri-Ghomi et al. 1999).

This chapter is organized in three sections. In Sec. 6.2 we present the computational model used to simulate the tensile debonding of two polymer bulks glued together by connector chains at the interface. The section starts with a short presentation of the potentials governing the interactions between the polymer chains. Then we describe the generation and pre-equilibration of the polymeric system prior to the tensile pull. Section 6.3 contains our results and discussion regarding the effects of different internal and external parameters on the adhesion strength. The chapter ends with the conclusions in Sec. 6.4.

6.2 Model and simulation method

We perform molecular dynamics (MD) simulations of a system formed by two polymer bulk samples situated on top of each other and bonded together by connector chains. The two polymer bulks are placed in separate MD boxes and do not interact with each other directly. The connector chains are located at the interface, penetrate into the two simulation boxes and interact with the bulks via an attractive Lennard-Jones potential, realizing in this way the adhesion. During the MD run, the upper box is pulled upwards, as a whole, at constant speed while the lower box in kept fixed and we measure the work necessary to break the adhesion by monitoring the forces in the connector chains.

In the current study, only the case of tensile debonding is considered for which the two polymer bulks are pulled apart along the vertical direction perpendicular to the interface. A separate future study is needed for the case of shear pull where the two bulks slide horizontally with respect to each other.

The polymer bulks are modeled as 3D ensembles of interacting chains placed in two separate simulation boxes: M chains with N beads per chain, at a bead number density $\rho = 0.85\sigma^{-3}$ for each polymer bulk. The connector chains cross the interface

between the two simulation boxes: m chains with n beads per chain (split in blocks of n_i beads), at a variable areal density of the connectors Σ. Special attention is paid to number of stitches s made by connectors at the interface and to its influence on the adhesion strength. The initial generation of the connectors between the two bulks, prior to the tensile debonding, is carefully controlled: all connectors have the same number of stitches that can vary from one to four as represented in Fig. 6.1.

6.2.1 Interaction potentials

For each polymer chain (either inside the bulks or being a connector) we use a coarse-grained representation based on the Kremer-Grest (1990) model, extended to account for stiffness along the chain backbone (Bulacu and Van der Giessen 2005).

The two polymer bulks are confined in the pulling direction (Z) perpendicular to the interface. This is achieved by using a repulsive interaction between the bulk beads and the walls of the MD box perpendicular to Z. Each bead from the polymer bulk interacts with the upper and lower walls of its simulation box via an integrated 3-9 Lennard-Jones potential:

$$V_{\mathrm{LJ}}^{\mathrm{wall}}(z) = \frac{2\pi\varepsilon^{\mathrm{wall}}}{3}\left[\frac{2}{15}\left(\frac{\sigma^{\mathrm{wall}}}{z}\right)^{9} - \left(\frac{\sigma^{\mathrm{wall}}}{z}\right)^{3}\right], z < z_{\mathrm{cutoff}}^{\mathrm{wall}}. \tag{6.1}$$

Its graph is represented in Fig. 6.3 and the values of $\varepsilon^{\mathrm{wall}}$ and σ^{wall} are given in Table 6.1 together with all the other parameters of the interaction potentials used in our simulations.

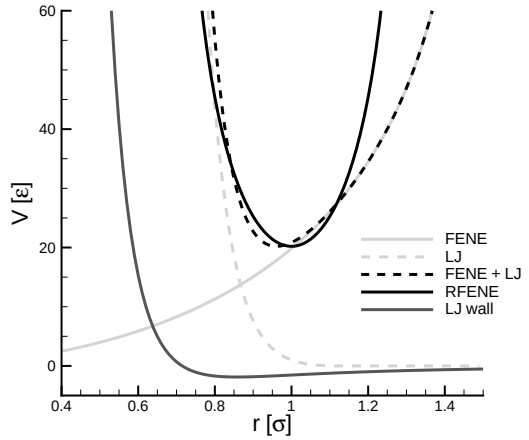

Figure 6.3: *Potentials used for the interaction between the bulk chains and the walls (LJ integrated wall – dark gray line) and between two connected beads (FENE+LJ for the chains in the bulks – black dashed line, and reflected FENE for the connectors – black solid line).*

parameter	MD units
Lennard-Jones length σ	1
Lennard-Jones minimum energy ε	1
Lennard-Jones cut-off distance r_{cutoff}	$(2)\sqrt[6]{2}$
Lennard-Jones wall length σ^{wall}	1
Lennard-Jones wall energy $\varepsilon^{\text{wall}}$	0.85
Lennard-Jones wall cutoff distance $z^{\text{wall}}_{\text{cutoff}}$	0.85
FENE elastic constant k	30
Maximum bond elongation (FENE) R_0	1.5
RFENE elastic constant k_{r}	50
Maximum bond elongation (RFENE) R_{r}	1.3
Bending constant k_θ	25
Bending equilibrium angle $\cos\theta_0$	-0.333
Torsion constant k_ϕ	1
Torsion polynomial coefficients:	
a_0	3.00
a_1	-5.9
a_2	2.06
a_3	10.9

Table 6.1: *Parameters used in simulations (in MD reduced units).*

This LJ-wall potential mimics the interaction of the particles from the bulks with an infinite half-space uniformly filled with 6-12 LJ (Eq. (6.2)) particles (Sides et al. 2002, Sides et al. 2004). This interaction is not felt by the connector beads. The bulk beads are kept strictly inside the simulation box on the Z direction by the repulsive force with the box walls. This interaction is essential in allowing the construction of the adhesion interface as the system must be confined to a finite range along the Z axis. This is in contrast with the periodic boundary conditions used on the X and Y axes, simulating a continuum in these two directions. The LJ-wall potential will also prevent the bulk particles from being pulled outside the simulation box on the Z direction as they are engaged by the connector chains during the debonding simulation. In Fig. 6.4 an example of a simulated polymer bulk is given to emphasize the effects of the LJ walls.

The bond between two successive beads along the chain is modeled differently for the bulks and for the connectors. In the polymer bulks, two connected beads interact through the combination of two potentials: the repulsive Lennard-Jones (LJ) potential

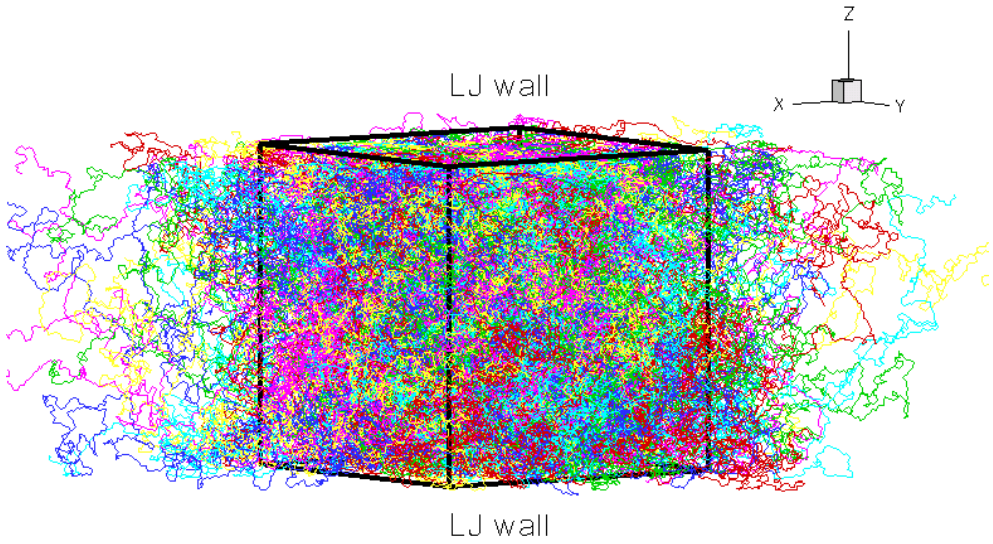

Figure 6.4: *An example of a simulated polymer bulk ($M = 75$ chains with $N = 500$ beads per chain). In the Z direction two LJ-wall potentials are used to confine the polymer beads. In X and Y directions periodic boundary conditions are employed. Their effect is not represented in the figure by re-introducing the outside beads back in the simulation box. Two boxes like this are glued together on the Z direction by connector chains.*

plus the finite extensible non-linear elastic (FENE) potential:

$$V_{\mathrm{LJ}}(r_{ij}) = 4\varepsilon \left[\left(\frac{\sigma}{r_{ij}} \right)^{12} - \left(\frac{\sigma}{r_{ij}} \right)^{6} + \frac{1}{4} \right], r_{ij} < r_{\mathrm{cutoff}}, \tag{6.2}$$

$$V_{\mathrm{FENE}}(r_{ij}) = \begin{cases} -\frac{1}{2} k R^2 \ln \left[1 - \left(\frac{r_{ij}}{R} \right)^2 \right], & r_{ij} \leq R_0 \\ \infty\,, & r_{ij} > R_0\,. \end{cases} \tag{6.3}$$

In it important to observe that the FENE+LJ combination is asymmetric with respect to the equilibrium bond length $b_0 = 0.96\sigma$ (the black dashed line in Fig. 6.3). Bonds are allowed to extend more easily than to compress. As a consequence, the average bond length in the normal state is slightly larger than the equilibrium bond length b_0. Overall, the bonds are slightly stretched and the average tension in the chains is negative, rather than zero. This systematic effect can be allowed for the polymer bulks, but it must be eliminated for the connector chains, because we will measure the adhesion strength by monitoring the tension induced in the connectors by the applied tension.

A symmetrized potential is thus needed to model the bonds between successive beads on the connector chains. For this purpose, we reflect the FENE potential around

the equilibrium bond length $b_0 = \sigma$. The reflected FENE (RFENE) potential

$$V_{\mathrm{RFENE}}(r_{ij}) = \begin{cases} -0.5 k_r R_r^2 \ln \left\{ \left[1 - \left(\frac{r_{ij}}{R_r} \right)^2 \right] \left[1 - \left(\frac{2\sigma - r_{ij}}{R_r} \right)^2 \right] \right\}, & r_{ij} \leq R_r \\ \infty, & r_{ij} > R_r \end{cases} \tag{6.4}$$

controls, in a symmetric manner, both the elongation as well as the compression of the polymer bonds, on either side of the equilibrium bond length $b_0 = \sigma$. Two parameters must be set for the reflected FENE potential: the maximum elongation R_r and the elastic constant k_r. The values given in Table 6.1 were chosen such that the RFENE potential overlaps as much as possible with the FENE+LJ potential over the active range of bead distances in the neighborhood of the equilibrium bond length (see Fig. 6.3).

The bonds from the bulks will be modeled using the FENE+LJ potential in order to remain comparable with our previous studies of polymer melts. The bonds from the connector chains will, however, be modeled using the RFENE potential, which is symmetric and allows us the measure the adhesion strength by monitoring the connector tension without any systematic bias.

An important aspect in this study is the control of chain stiffness. The stiffness along the chain backbone is enhanced by using a bending potential V_{B} and a torsion potential V_{T} acting on three, respectively four, consecutive connected beads. The bending potential maintains the angle between adjacent pairs of bonds to the equilibrium value chosen $\theta_0 = 109.5°$:

$$V_{\mathrm{B}}(\theta_i) = \frac{1}{2} k_\theta (\cos\theta_i - \cos\theta_0)^2. \tag{6.5}$$

The torsion potential constrains the dihedral angle ϕ_i to three possible equilibrium values $\phi = 180°$ (trans), $\phi = 60°$ (gauche$^+$) and $\phi = 300°$ (gauche$^-$). We use a form of the torsion potential that depends also on bending angles. This makes the potential and its corresponding force to cancel when the dihedral angle ϕ becomes undefined (two consecutive bonds align):

$$V_{\mathrm{T}}(\theta_{i-1}, \theta_i, \phi_i) = k_\phi \sin^3\theta_{i-1} \sin^3\theta_i \sum_{n=0}^{3} a_n \cos^n \phi_i. \tag{6.6}$$

The way in which the bending and torsion angles are defined has been described in Fig. 2.3. These potentials have been used also in the previous chapters and thoroughly analyzed their influence on the static and dynamic properties of polymer melts (Bulacu and Van der Giessen 2005, Bulacu and Van der Giessen 2007).

Because geometric singularities are gracefully eliminated without the need for rigid constraints, these continuous potentials have clear computational benefits allowing the stable simulation of large systems. In this chapter, the influence on the adhesion strength

of bending and torsion potentials, acting on connector chains, is investigated. The potentials V_{B} and V_{T} are applied to the bulk chains in all our experiments. While the bulk chains are in the same stiffness state only the stiffness of the connector chains will be varied in different simulation runs.

The bulks will be kept in the same reference state below the glass transition temperature, only the stiffness of the connector chains will be changed in different simulation runs to see its effect on adhesion strength.

Unconnected beads interact via the LJ potential (Eq. (6.2)). Two different cutoff distances are used: the interaction between two beads from the bulk is purely repulsive with $r_{\mathrm{cutoff}} = \sqrt[6]{2}$, while the interaction between a connector bead and a bulk bead includes also the attractive part of the LJ potential, $r_{\mathrm{cutoff}} = 2\sqrt[6]{2}$. The cutoff distance is therefore used to differentiate the bulk-bulk interaction (repulsive LJ) from the connector-bulk interaction (attractive LJ). This distinction is important: the repulsive LJ interaction induces a uniform bead distribution inside the two polymer melts, while the attractive LJ interaction between the connectors and the bulks is essential in realizing the adhesion. The connector-connector interaction is also repulsive LJ, similar to the interaction between beads within the two polymer bulks.

The strong interaction between connected beads (FENE+LJ in the bulks and RFENE in the connectors) coupled with the excluded volume interaction between unconnected beads (repulsive part of LJ potential) prevents the chains from crossing each other and yields entangled polymer ensembles (Kremer and Grest 1990). The chain motion is restricted by the entanglement with the other chains from the ensemble.

6.2.2 Sample preparation

Prior to the debonding simulations, a careful preparation of the samples is required. The polymer chains from the bulks are generated as random walks with constraints for the bond lengths, bending and torsion angles around their equilibrium values needed for the specific potentials (Bulacu and Van der Giessen 2005). For all simulations referred here the bulk chains have bending and torsion stiffness: $k_\theta = 25\varepsilon$, $k_\phi = 1\varepsilon$. Supplementary constraints are imposed during chain generation to keep the beads inside the simulation box in the Z direction. This is achieved by rejecting those random moves that come closer to the box walls than a chosen safe distance.

The connector chains are generated such that they have a predefined conformation at the interface – with a certain number of stitches and a certain number of beads between the stitches. To obtain such controlled connectors we separately produce tails which start from a point on the interfacial plane and loops which start and stop on the interfacial plane using a random walk procedure similar to that used for the bulk chains. The tails and loops (individual connector blocks) are then concatenated to obtain connectors

with the desired number of stitches, cf. Fig. 6.1. Mostly the generated connectors have equal blocks between the stitches: $n_{\mathrm{b}} = n/(s+1)$ where s is the number of stitches. For special cases the connector blocks are not equal and the connector is explicitly described (e.g. $n_1 : n_2 : n_3 : n_4$ for a three stitch connector) or the blocks have completely random lengths.

The two polymer bulks are placed on top of each other and the preformed connectors are uniformly distributed at the interface according the desired areal density of the connectors Σ. The successive blocks (tails or loops depending on s) of each individual connector chain are immersed alternately in the two polymer bulks. The resulted intertwining between connector chains and bulk chains, which cannot cross each other, consequently establishes the adhesive junction.

Our study is restricted to low connector areal densities for which is assumed that the connectors do not interact with each other and consequently the initial random walk generation is appropriate. This regime was named the "mushroom" regime by Raphaël and de Gennes (1992) and is valid for the value of $\Sigma \leq 0.008$ (Sides et al. 2001, Sides et al. 2002), predominantly used in this study. For the situation of high connector areal density ("brush" regime) there is no clear evidence of the how the connectors are placed at the interface. Still special generation methods have been proposed (Sides et al. 2004, Terzis et al. 2000a, Terzis et al. 2000b).

A packing procedure is used after generation to make the initial distributions of particles in the two simulation boxes as uniformly as possible: while the connectors are kept fixed, small random moves are applied to the bulk chains (treated as rigid objects) with the aim to reduce the variance of the local bead density within the two simulation boxes.

Two short MD stages are employed next in order to bring the whole system to equilibrium: a slow push-off stage uses capped LJ potentials to eliminate the bead overlaps, followed by a brief MD run when the full potentials are turned on and the system is taken to the desired temperature (Auhl et al. 2003, Bulacu and Van der Giessen 2005).

6.2.3 Tensile debonding MD simulation

In the current work, we study how the connector chains are forced to disentangle when the two bulks are pulled apart. It is assumed that the connector chains do not break, but slip out from the bulks in a viscous process. If a bond length exceeds a maximum value of 1.3σ, the polymer chain is considered broken and the simulation stops. The adhesion strength will be computed by integrating the tension appearing in the connectors chains as they are forced to follow a reptation motion induced by the growing separation between the two polymer bulks.

Tensile debonding is achieved by moving up the top bulk as a whole (together with

its walls) at a constant pull velocity $\mathbf{v}_{\text{pull}}$. The majority of experiments are performed at $v_{\text{pull}} = 0.1\sigma/\tau$. The fracture is complete when there is no connector with beads located inside both simulation boxes and thus no force is transmitted across the interface.

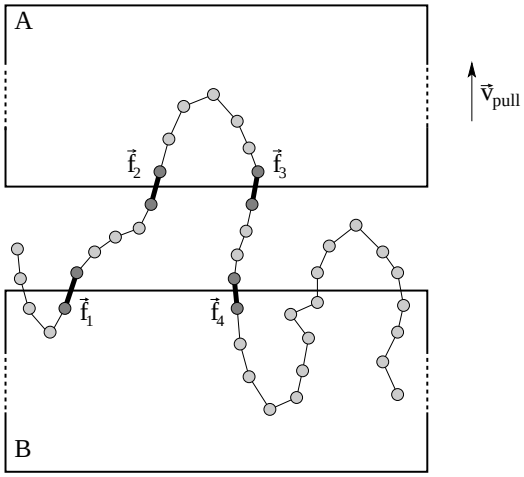

Figure 6.5: *An example of a connector crossing the two melts. Only the thick bonds are considered for computing the transmitted force F.*

During the debonding simulation we determine the work necessary to separate the two bulks (A and B). The work W is computed as the time-integral of the tension force that is induced in the connector chains by the pulling action. For computing the tension force F we chose to consider half of the sum of the bond forces (RFENE) for all the connector bonds that cross the lower boundary of melt A and, subsequently, the upper boundary of melt B, or vice-versa (see Figure 6.5):

$$F(t) = \frac{1}{2} \sum_i \mathbf{f}_i(t) \cdot \mathbf{e}_z \tag{6.7}$$

where $\mathbf{e}_z$ is the unit vector on Z direction and the sum goes over all pair of bonds that cross the two simulation boxes in sequence (there are four such bonds in Figure 6.5). The $1/2$ factor from the calculation of F is used because in fact two equal tensions on both bulks are summed.

The instantaneous tensile power at time t per unit area, needed to keep the upper bulk in motion with the velocity v_{pull}, is given by

$$w(t) = F(t) v_{\text{pull}} / A \tag{6.8}$$

where $A = l_{\text{box}}^2$ is the interfacial area (l_{box} the box length).

The work needed to separate the two simulation boxes up to the time t becomes:

$$W(t) = \int_0^t w(t')dt' \tag{6.9}$$

Measuring the work of adhesion as the time-integral of the total tension induced in the connector chains by the pulling action is an important choice we decided to make if our computational experiments. We emphasize the fact that all other simulation parameters will ultimately have an effect on the tension appearing in the RFENE bonds of the connectors. The connectors will be disentangled from inside the two bulks under the action of this tension force and, as we will see further, the results fully reflect the nature of this reptation process.

Figure 6.6 shows an example of the time evolution during debonding for the force F and the work of adhesion W. The dependence of F with simulation time can be translated in a traction-separation law to be used in subsequent continuum modeling. The adhesion strength G is evaluated as the plateau value from W versus t that appears at t_{D} – the total debonding time.

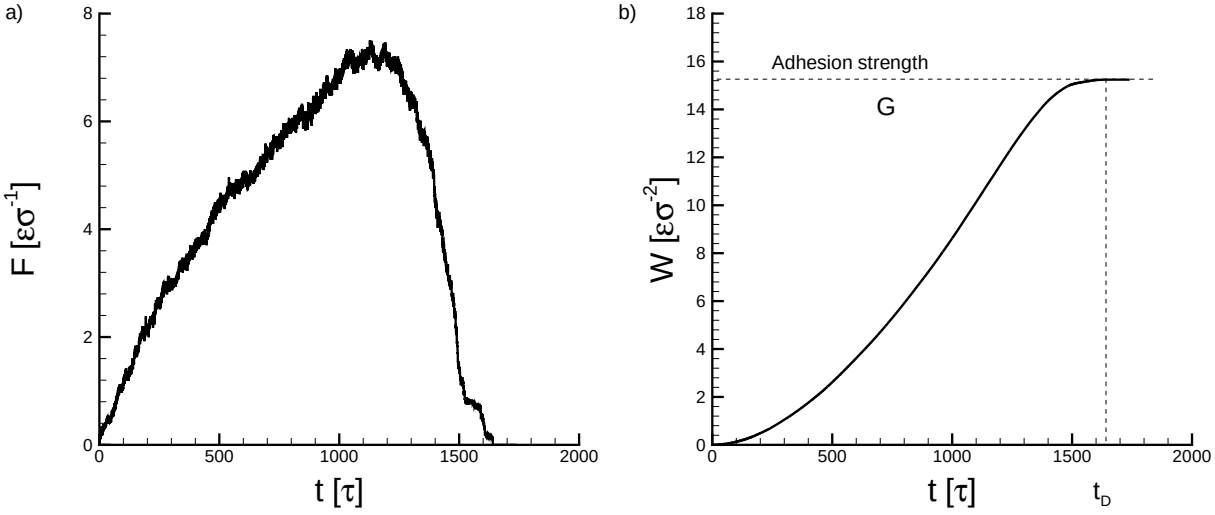

Figure 6.6: *Time dependences of total force F transmitted between the two polymer bulks (a) and the work W spent during debonding (b). The adhesion strength G is assumed the plateau value of W that appears at t_{D} – the total debonding time (one-stitch connectors with $n = 200$).*

The MD runs are performed at constant temperature T and volume V (for each simulation box). We chose for constant-volume simulations instead of constant-pressure to avoid the supplementary tensions induced in the system by volume adjustment.

The temperature is kept constant by coupling the system to a heat bath: the friction coefficient is $\Gamma = 0.5\tau^{-1}$ and the strength of the Gaussian white-noise force is $6k_BT\Gamma$. All the experiments, except the ones in which the temperature dependence of the adhesion strength is investigated, are performed at $T = 0.3\varepsilon/k_{\mathrm{B}}$. This value was chosen to be below the glass transition temperature of bulk systems with RIS chains, estimated as $T_{\mathrm{g}}^{\mathrm{RIS}} = 0.7\varepsilon/k_{\mathrm{B}}$ by Bulacu and Van der Giessen (2007).

The equations of motion are integrated using the 'velocity-Verlet' algorithm (Swope et al. 1982) with a time step $\Delta t = 0.01\tau$. A boxing scheme is used for the efficient implementation of the LJ interactions.

Results will be presented from simulations with different connector chain lengths $n \leq 500$ and areal densities Σ, at different pulling velocities v_{pull}. The connector chain stiffness will be varied and its effect on adhesion strength will be analyzed. The simulation box size was chosen such that the connectors do not come close to the walls opposite to the interface. In each case, the length of the bulk chains was $N = 500$, while the number of chains M was computed to obtain the desired bead density ($\rho = 0.85\sigma^{-3}$) inside the simulation boxes. The final results are averaged over approximative 20 independent experiments to account for the variation caused by the random distribution of the connectors at the interface.

Figure 6.7 shows a simplified flowchart of the MD code used for adhesive fracture simulations.

An average simulation time was $10^5\tau$ and required approximately 100 hrs of computation on a 2.8 GHz/1 GB Pentium 4 processor.

6.3 Results and discussion

In this section we present our simulation results and start by looking at some graphical representations showing the evolution of the adhesion system during the debonding pull. Figure 6.8 presents three snapshots (initial, middle and final) from a simulation of a system with one-stitch connectors (of length $n = 150$) placed at the interface. As the interface widens, the connectors are first extended, and then parts of them are gradually pulled-out from the bulks into the empty region between the two simulation boxes.

To obtain a complete separation, all the connectors must be outside from at least one polymer bulk. Since the interaction between the connectors and the two bulks is identical, and usually the connectors are symmetric, the slippage of the chains has no preferred direction.

To gain a better understanding of how the connectors act during debonding, the histograms of bonds, bending angles and torsion angles are extracted and included in Fig. 6.8. The histograms are collected by computing all the bond lengths, bending and torsion angles along the entire connector chain, irrespective of their location (whether inside or outside the bulks). Observing the histograms of the bond lengths, we can see that, as debonding progresses, the bonds are more and more stretched from the equilibrium value of σ up to a maximum of about 20% elongation. This effect is the basis for computing the work of adhesion by integrating the tensions appearing in the connector bonds elongated due to the pulling action. The bending angles evolve towards values

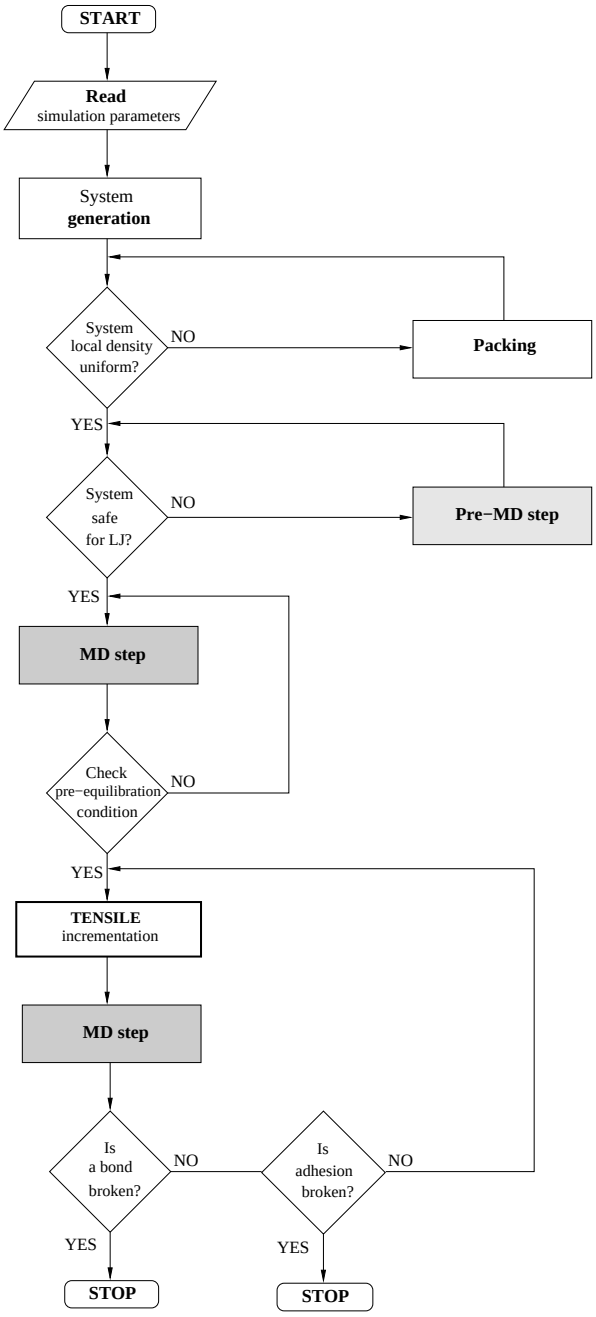

Figure 6.7: *Schematic representation of the program used for simulation of the fracture of adhesion between two polymer bulks reinforced with connector chains. The MD step includes also the "on the fly" analysis (e.g. the calculation of the debonding work and the extraction of specific histograms).*

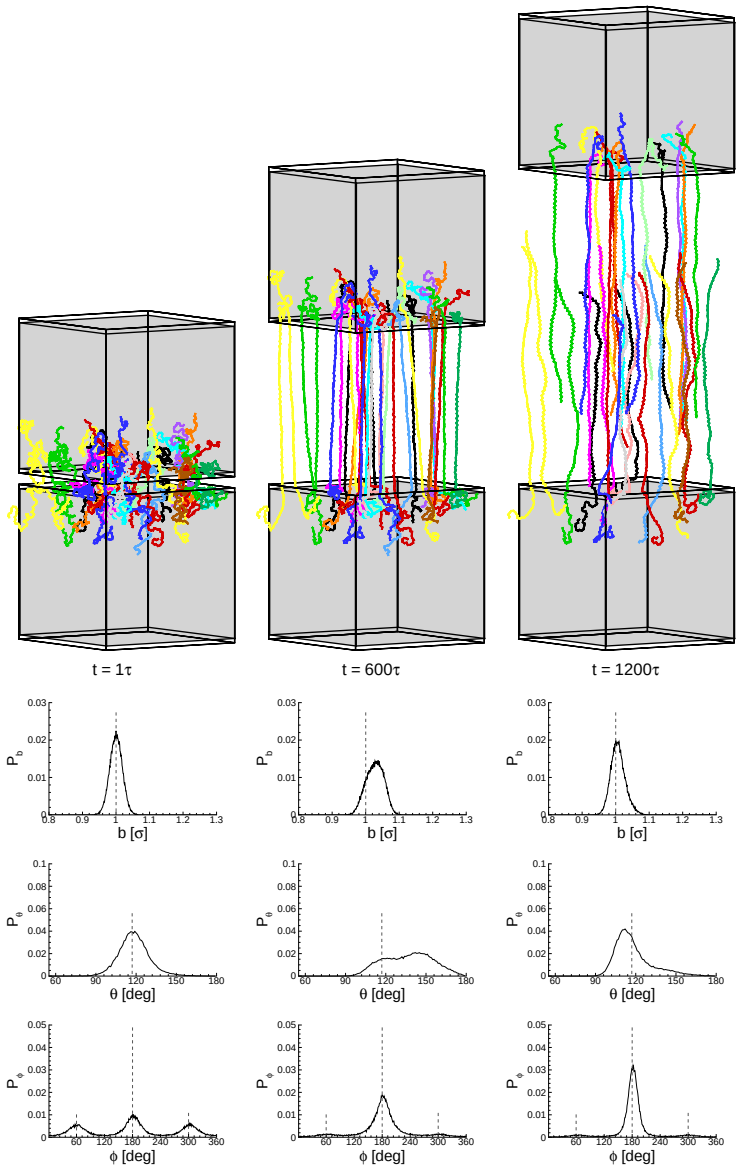

Figure 6.8: *Three snapshots from the tensile debonding simulation of a system with* $m = 30$ *one-stitch connectors with* $n = 150$ *beads per connector at an areal density* $\Sigma = 0.008\sigma^{-2}$*. The elapsed time is indicated below each figure. For clarity, the polymer chains from the two bulks are not shown. Below each snapshot, we represented the corresponding histograms for the bond lengths* b*, bending angles* θ *and torsion angles* ϕ *of the connector chains.*

closer to $180°$, while, in the distribution of torsion angles, the *gauche*$^+$ ($\phi_0 = 60°$) and *gauche*$^-$ ($\phi_0 = 300°$) states disappear leaving a dominant *trans* state ($\phi_0 = 180°$). We found no difference in the moment of onset and speed of these modifications appearing in the three histograms.

As the connectors are completely pulled out from one bulk and do not transfer tension anymore, the bond lengths and bending angles return to their equilibrium values. On the contrary, the torsion angles remain in the *trans* state, because the energy barrier to the *gauche* states cannot be surpassed due to the very low temperature.

A more complex behavior is observed for long connectors ($n = 500$), as shown in Figure 6.9. Not all the bonds along the chain deform uniformly: some are visibly elongated, while others remain unstressed, thus giving rise to the two separate peaks in the bond length histogram. By comparing with previous figure, we observe that the bonds that are stretched are, in fact, subjected to a larger tension and deviate more from the equilibrium value σ. This will lead to a larger integrated work of adhesion. The tension acts on the portion of the connector chains situated between the two bulks. For this region, the bending angles open to 180°, giving rise to the sharp peak in the θ histogram from Figure 6.9. When the bending angles are close to 180°, the torsion potential vanishes and, as a result, the histogram of dihedral angles flattens. This behavior is observed also for shorter chains when the pull velocity is increased.

6.3.1 Influence of connector chain architecture on adhesion strength

In this subsection we will start by showing that the adhesion strength depends on the connector length as n^2. This scaling law remains valid also when the connector stiffness is changed or when the number of stitches formed by the connectors at the interface is increased. The $G \propto n^2$ dependence is directly related to the nature of the polymer chain motion inside a dense entangled ensemble of other polymer chains. Let us make some simple theoretical considerations and then show numerical results to support this scaling law.

The force field used in our simulations does not allow the chains to cross each other and this results in an entangled system (Kremer and Grest 1990, Bulacu and Van der Giessen 2005). Inside polymer melts, if the chains are long enough, they are confined to move along a "tube" determined by the restrictions due to the neighboring chains. Reptation theory (de Gennes 1979, Doi and Edwards 1989) predicts that chain self-diffusion in melt is retarded and the diffusion coefficient D scales as N^{-2}, where N is the chain length. In the reptation "tube" however, the chain diffuses like a Rouse particle and this one-dimensional self-diffusion scales as N^{-1}.

The connectors are pulled out from the bulks in a similar manner, during the tensile debonding of the two glassy polymer bulks. They are forced to creep along the tube, in an accelerated reptating manner. Next we attempt a simple theoretical description of this phenomenon, following Evans (1987).

If we consider a part of a chain of length l (with n_1 beads and bond length b) immersed in a polymer bulk, the force required to extract it must overcome Stokes's drag

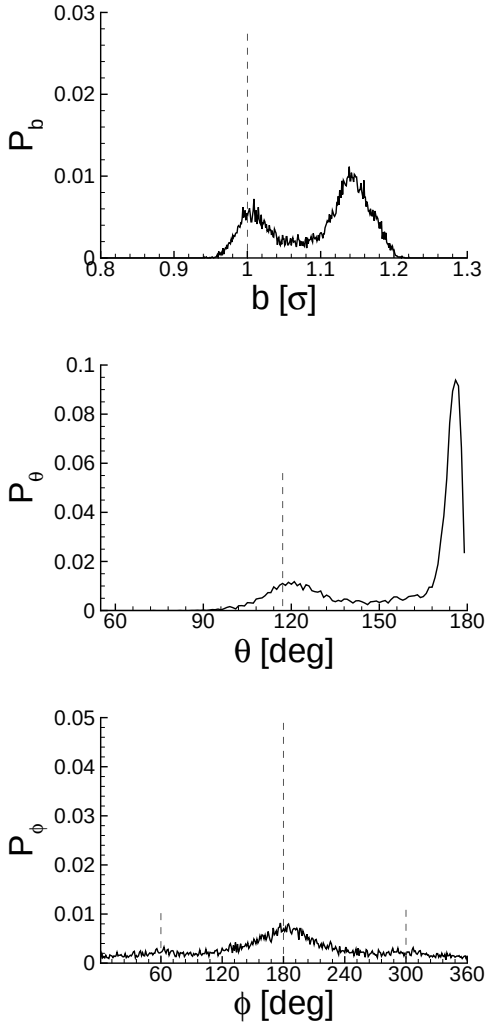

Figure 6.9: *Histograms of the bond lengths b, bending angles θ and torsion angles ϕ for a system with long one-stitch connectors with $n = 500$ beads.*

force:

$$f = \gamma v \tag{6.10}$$

where γ is the drag coefficient and v is the pulling velocity. The coefficient γ may be considered the inverse of the mobility and, according to Einstein's relation, $\gamma = k_{\mathrm{B}}T/D$. If we assume that the polymer chain is pulled out along a tube determined by the neighboring chains, the diffusion coefficient D along the tube may be replaced with $D = D_0/n_{\mathrm{l}}$ according to the Rouse model, D_0 being the bead diffusion coefficient. In this way, Eq. (6.10) becomes:

$$f = \mu_0 l v, \tag{6.11}$$

where $\frac{k_B T}{D_0 b}$ has been replaced with μ_0 that can be regarded as a bead friction coefficient. Consequently, the total work required to completely pull out an entire connector chain of length L (n beads) is given by:

$$w = \int_{l=0}^{l=L} \mu_0 l v \, dl = \frac{\mu_0}{2} L^2 v = \frac{\mu_0 b^2}{2} v n^2 \tag{6.12}$$

This dependence $w \propto n^2$ for the pullout regime relies on reptation theory and has been deduced in several other approaches for glassy polymer fracture or reinforced interfaces (Prentice 1983, Evans 1987, de Gennes 1989, Xu et al. 1991).

Washiyama et al. (1993) have demonstrated this scaling to be a good fit to the data obtained experimentally for a PS-PVP interface reinforced with PS-b-PVP connectors in a pure pullout regime (no crazing).

Figure 6.10 shows the time evolution during debonding of the work of adhesion for one-stitch systems with different connector length. Obviously, longer connectors require more time to full debonding and this yields larger accumulated work.

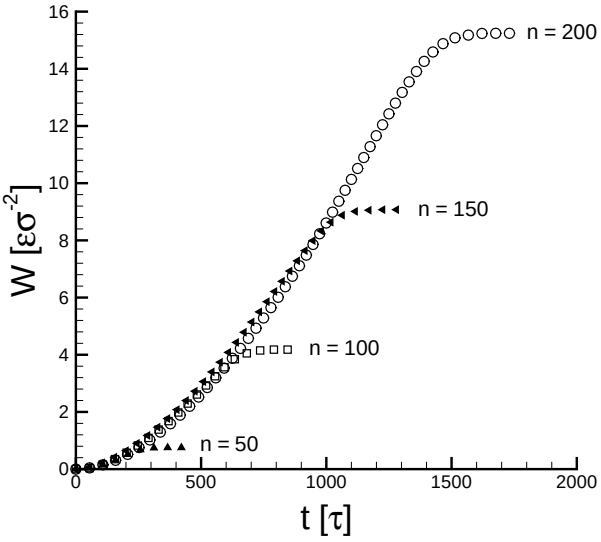

Figure 6.10: *The time evolution of the work of adhesion for the one-stitch case with different connector lengths at areal density* $\Sigma = 0.008\sigma^{-2}$.

The plateau of W reached after the complete separation gives the adhesion strength G. Figure 6.11 shows the G versus n dependence for several systems in which the number of stitches was varied. We obtained regression coefficients for $G \propto n^2$ in the vicinity of 0.98.

Besides $G \propto n^2$, Figure 6.11 shows also the effect that the number of stitches has on adhesion strength. This is an important research question and several experimental

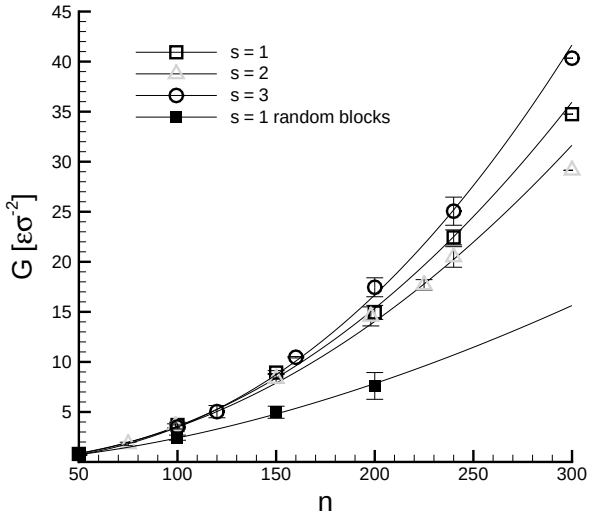

Figure 6.11: *The adhesion strength versus the number of beads per connector, for different number of stitches.*

studies (e.g. Dai, Dair, Dai, Ober and Kramer 1994, Brown et al. 1993) have been done by replacing the di-block connectors that form a single stitch at the interface with multi-block connectors that form multiple stitches. Due to the fact that the connectors make multiple excursions across the interface, the areal density of stitches differs from the areal density of connectors. In experiments, the connector density can be controlled, but the stitch density remains uncertain, despite the preformed chemical structure (e.g. tri-block).

In computer simulation, however, it is possible to completely control the initial configuration of the connectors at the interface – both the number of stitches and the number of beads in each block between the stitches. Our procedure for generating the connectors allows for an extensive study of the influence of the number of stitches on the adhesion strength, at constant connector areal density as well as at constant stitch areal density.

Figure 6.12 shows the last snapshot at complete tensile separation of different systems in which the number of stitches s was varied, as illustrated in Fig. 6.1. In the two-stitch situation, Fig. 6.12a, most of the connectors remain attached to the upper bulk after fracture since the main polymer disentanglement in this particular situation happened for the tails situated in the bottom bulk. For the three-stitch case, the partition of connectors is more balanced between the two bulks due to the symmetry of the initial conformation. In the case $s = 4$ shown in Fig. 6.12c most chains stick to the bulk in which they have the central loop and the tails at the beginning of the simulation (please refer to the last panel in Fig. 6.1).

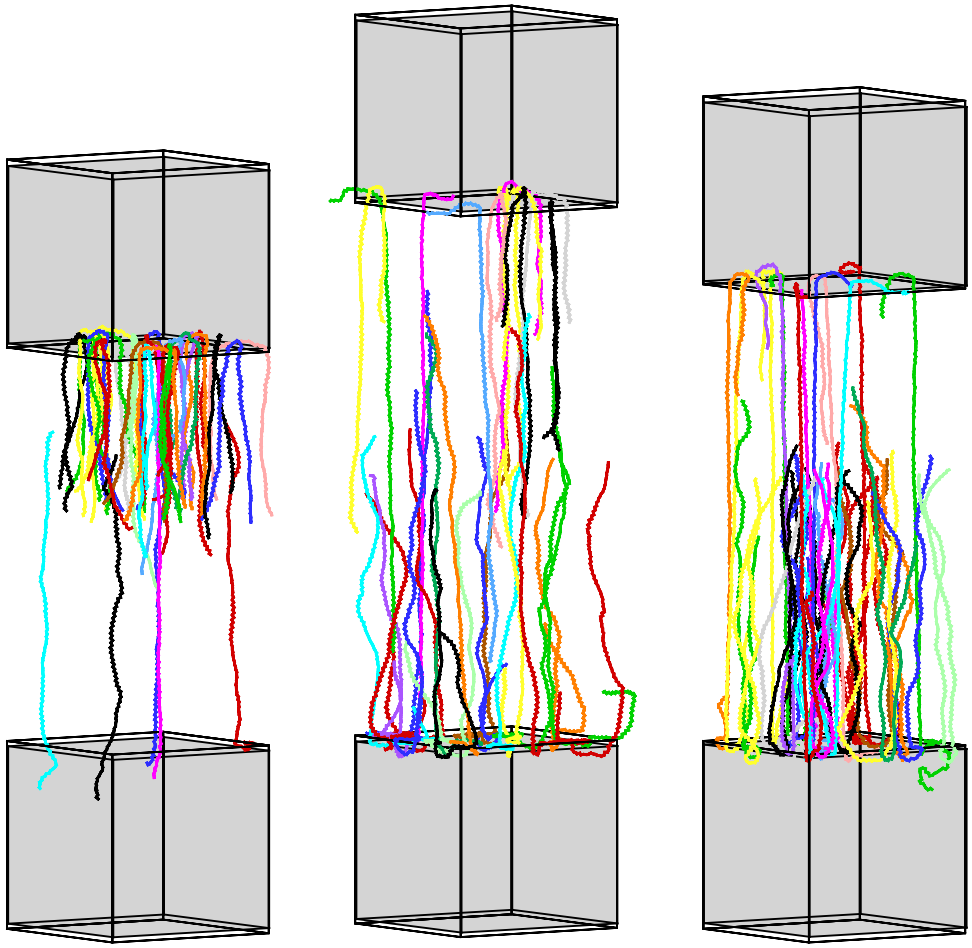

Figure 6.12: *The last snapshot from tensile debonding simulations for systems with (a)* $s = 2$*, (b)* $s = 3$*, and (c)* $s = 4$ *stitches at the interface. All the systems have the same number of connectors* $m = 30$*, with equal blocks between stitches* $n_\mathrm{b} = 50$ *(*$n = n_\mathrm{b}(s+1)$*). The connector areal density was constant* $\Sigma = 0.008\sigma^{-2}$*.*

The number of stitches does not change the scaling $G \propto n^2$ (see Fig. 6.11), however it influences the adhesion strength and this effect is better depicted in Fig. 6.13.

When the total length of the connector chain is kept constant, only a moderate increase in G with the number of stitches is observed. As the number of stitches increases, each connector block becomes shorter. A peculiar situation occurs for $s = 2$, where we observe that adhesion is weaker than for the one-stitch case. A possible explanation is that the tails of the two-stitch connector are shorter and consequently easier to extract than the tails of the one-stitch connector. The increase in G due to the stitches is more pronounced for longer chains (see Fig. 6.11).

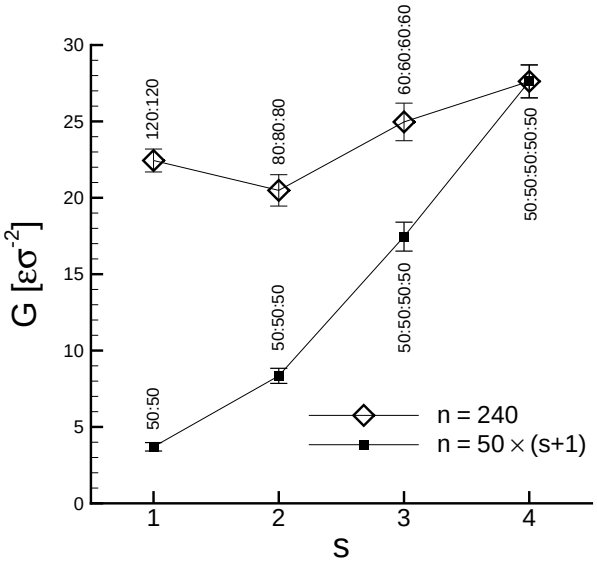

Figure 6.13: *Adhesion strength G versus number of stitches s. Two cases are considered: (1) constant connector length ($n = 240$ beads with equal blocks between stitches) – open symbols; (2) constant block length $n_\mathrm{b} = 50$ beads – solid symbols (the total length of the connector is $n = n_\mathrm{b}(s + 1)$).*

When the length of each block is kept constant and the total length of the connector multiplies with the number of stitches, the adhesion strength G grows significantly mainly due to the increased length of the chains (see Fig. 6.13).

The influence of the stitches on adhesion strength was investigated in computer simulation by only one other known study (Pickett et al. 1996, Pickett et al. 1997). The authors reported a larger improvement of the adhesion strength with the number of stitches for a constant chain length. The disagreement probably relies on the significant differences between the models: in that study, the bulks are modeled as 2D networks of fixed obstacles, the connectors have rigid bonds and they are grafted on the surface of one bulk during the pullout. Our system is much more fluid, because all our interactions are continuous and the connectors are free at the interface.

Our results, showing a moderate increase of the tensile work with the number of stitches at the same chain length, are in better qualitative agreement with experimental results that indicate random co-polymers connectors as "surprisingly effective in reinforcing polymer interfaces", but not better than di-block (one-stitch) connectors of the same length, at the same connector areal density (Creton et al. 1991, Brown et al. 1993, Char et al. 1993, Kramer et al. 1994, Dai, Dair, Dai, Ober and Kramer 1994, Benkoski et al. 2001). In the chain pullout regime, the external work goes mainly into the stretching of the connector molecules, which does not change dramatically from the one-stitch

case to the many-stitches cases (Ji and de Gennes 1993).

Another interesting comparison between reinforcement with one or two stitches can be done by considering the same areal density of stitches, instead of the same areal density of connectors, as in the experiments of Dai, Washiyama and Kramer (1994) and Dai et al. (1997). One can assume, as a first approximation, that a tri-block connector (forming two stitches) effectively consists of two "pseudo" di-block connectors obtained by cutting the loop into two equal parts (see figures from Table 6.2). We compare these two situations in the results given in Table 6.2. The total number of beads initially immersed in the two bulks is constant, while the chain connectivity is changed to reproduce the two situations. The connector areal density in the one-stitch case is doubled compared with the one for the two-stitch case. The results from Table 6.2 show that the coupling between the two polymer bulks is stronger for the two-stitch configurations.

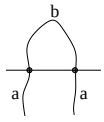		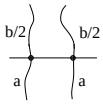	
$a : b : a$ $\Sigma = 0.008\sigma^{-2}$	G_2	$a : b/2$ $\Sigma = 0.016\sigma^{-2}$	G_1
$50 : 100 : 50$	9.78 ± 0.32	$50 : 50$	7.56 ± 0.19
$60 : 120 : 60$	13.59 ± 1.01	$60 : 60$	11.31 ± 0.53
$100 : 100 : 100$	29.14 ± 0.01	$100 : 50$	9.94 ± 0.87
$100 : 200 : 100$	36.95 ± 0.50	$100 : 100$	33.60 ± 2.02

Table 6.2: *Adhesion strength obtained for constant stitch areal density $\Sigma = 0.016\sigma^{-2}$. Two different chain architectures are considered: G_2 results from reinforcement with two-stitch polymer chains ($a : b : a$) with connector areal density $\Sigma = 0.008\sigma^{-2}$ and G_1 results from reinforcement with shorter one-stitch polymer chains ($a : b/2$) at a double connector density $\Sigma = 0.016\sigma^{-2}$.*

One important aspect that has also to be considered is how the beads of the connector are distributed among its blocks. Until now, we only considered blocks of equal length. In lower part of Figure 6.11, the graph with solid symbols shows the G versus n dependence obtained for one-stitch connectors with random block length. An evident decrease in adhesion strength is noticed, explained by the fact that the chain length effectively extracted from the bulks is shorter.

All experiments presented in this paper are performed in the "mushroom" regime: the number of connectors per unit interfacial area is relatively small and as a result the connectors do not interact with each other. Consequently, increasing the connector areal density is expected to have a linear effect on the adhesion strength since the effective interactions with the bulks increase monotonically (Xu et al. 1991, Creton et al. 2001). For the one-stitch case, this behavior is exemplified in Fig. 6.14: while the total work of

adhesion increases with the areal density of connectors, the time needed to completely separate the two bulks remains the same being related solely to the chain length.

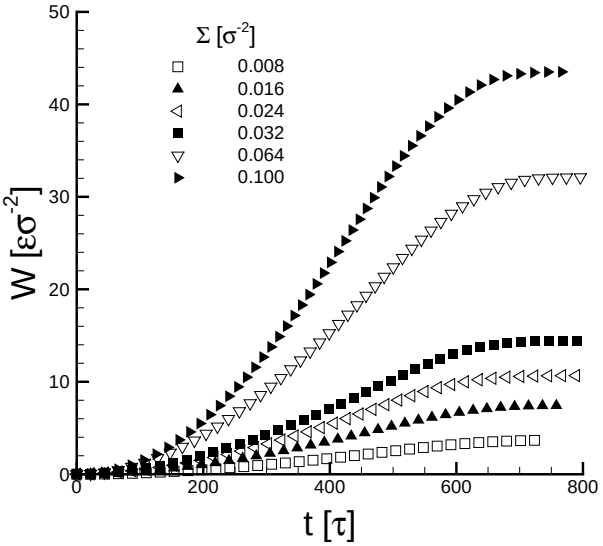

Figure 6.14: *Work of adhesion versus simulation time for different connector areal densities (one-stitch case with $n = 100$ beads per connector).*

The adhesion strength G estimated from the plateaus of Fig. 6.14 is shown as a function of Σ in Fig. 6.15, together with results obtained for the two-stitch case. Consistent with the basic premise of working in the "mushroom" regime, we observe that G scales as Σ^1, independent of the number of stitches at the interface.

In Figure 6.16, we compare the G versus n dependences for different connector stiffness. The default stiffness settings for our experiments were $k_\theta = 25\varepsilon$ and $k_\phi = 1\varepsilon$ both for the bulks as well as for the connector chains. Two modified stiffness cases were considered only for connectors: $k_\theta = 25\varepsilon$, $k_\phi = 0$ – no torsion potential acting on the dihedral angles, and $k_\theta = 0$, $k_\phi = 0$ – no bending, nor torsion potential (the stiffness is just intrinsic, resulting from the excluded volume interactions). The connectors were generated as RIS chains for all types of stiffness, to eliminate differences in the initial spatial conformation and retain only the effect due to the interaction potentials. For the specific fracture mechanism treated in this paper (pullout only), the connector stiffness seems to promote adhesion strength. The difference is noticeable between intrinsic stiffness and bending stiffness. The extra contribution due to torsion stiffness seems negligible, requiring further investigation.

This strengthening effect of connector chain rigidity in the pullout regime cannot be immediately translated into improved adhesion, since other fracture mechanisms may have a different sensitivity to chain rigidity. In particular, stiff long chains tend

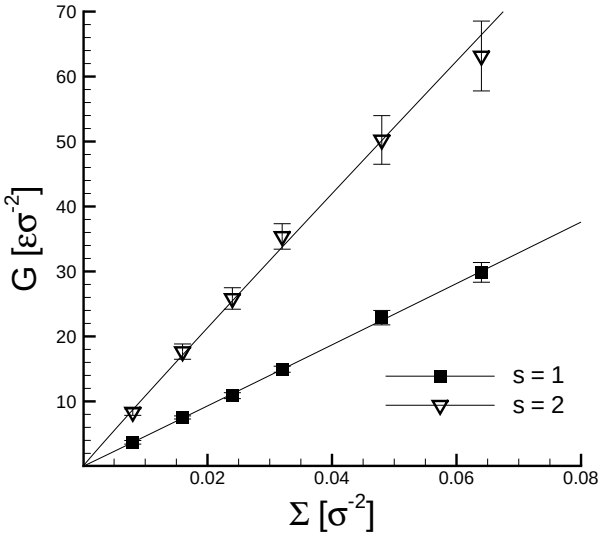

Figure 6.15: *Adhesion strength G as a function of connector areal density. Solid symbols represent the one-stitch case with $n = 100$ beads per connector (50:50) and open symbols represent the two-stitch case with $n = 150$ beads per connector (50:50:50).*

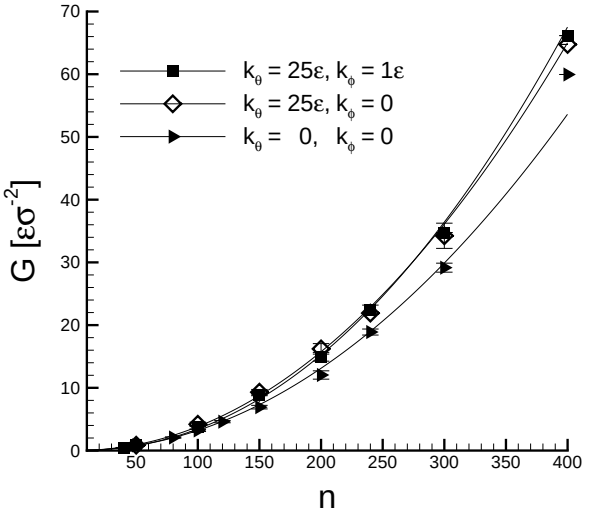

Figure 6.16: *Adhesion strength G versus connector length n for different chain stiffness. The connectors are all generated as RIS chains (random walks with constraints on the bending angles θ and dihedral angles ϕ). Here the one-stitch configuration was considered.*

to break easier than flexible ones. This explains why the effect of chain rigidity on adhesion (including multiple fracture mechanisms) is variable in experimental studies (Wu 1982, Voyutskii 1963) and simulations (Sides et al. 2002).

6.3.2 Influence of temperature and pull velocity on adhesion strength

In this sub-section, the influence of the external conditions during the debonding is investigating by performing simulations at different temperatures and pulling velocities.

Before starting, a clear distinction has to be made between the *joining* temperature at which the formation of the adhesive bonding takes place, and the *pulling* temperature at which the separation is performed. An increase in *joining* temperature is assumed to promote the adhesion strength due to the intensification of the diffusion process that leads to a deeper penetration of the connector chains inside the bulks. On the other hand, the *pulling* temperature determines the thermal motion in the system and facilitates the pulling-out of the connectors from the bulks and as a result the adhesion strength drops.

In this study, the equilibration before debonding is relatively short and temperature does not play a significant role in the final penetration depth. Hence, the effects observed in our simulations are mainly due to the *pulling* temperature.

Figure 6.17 presents the temperature dependence of the adhesion strength for systems with one-stitch symmetric connectors of lengths $n = 100$ and $n = 200$ beads per chain. The temperatures interval was chosen to embrace the glass transition temperature for the bulks ($T_{\mathrm{g}} \approx 0.7\varepsilon/k_{\mathrm{B}}$).

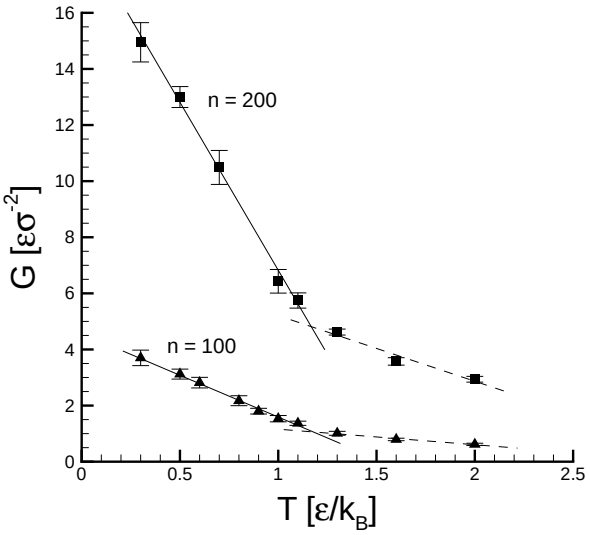

Figure 6.17: *Adhesion strength G versus temperature T for one-stitch connectors with $n = 100$ and $n = 200$ ($v_{\mathrm{pull}} = 0.1\sigma/\tau$).*

As expected, the total work of adhesion needed for a complete separation decreases as the temperature increases since the internal motion facilitates the extraction of the connector chains from the bulks. Similar trends have been reported based on computer

simulations in Refs. (Sides et al. 2001) and (Sides et al. 2002), and in experiments for PMMA-PS interfaces reinforced with PMMA-PS connectors (Brown et al. 1993).

As shown in Figure 6.17, the temperature dependence is strongly influenced by the connector length and by the temperature interval itself. The data shows two distinct temperature intervals, separated at approximately $T = 1.2\varepsilon/k_{\mathrm{B}}$, where the slope of G versus T dependence changes. At low temperatures, the variation of G is larger because the thermal fluctuations are more localized for a system in the glassy state. The value $T = 1.2\varepsilon/k_{\mathrm{B}}$ might be considered the glass transition temperature of the whole adhesion system. This temperature is larger than $T_{\mathrm{g}} = 0.7\varepsilon/k_{\mathrm{B}}$ specific to the equilibrated bulk phase due to the high pulling rate $v_{\mathrm{pull}} = 0.1\sigma/\tau$ at which our debonding simulations are performed.

We will now analyze how adhesion strength G depends on the pulling velocity v_{pull}. To the best of our knowledge, this is the first time when the relationship G versus v_{pull} is systematically investigated in MD simulations of tensile fracture of two polymers reinforced with connector chains at the interface. The experimental evidence about the rate effects on adhesion is still contradictory: Kramer et al. (1994) and Passade et al. (2000) report a clear dependence of the work of adhesion in glassy polymers on the pulling velocity, while Washiyama et al. (1993) shows that the adhesion strength is only slightly modified with velocity. We note that in the study presented here the pulling velocities used in MD simulations are orders of magnitude higher than the ones used in experiments (Sides et al. 2004). Figure 6.18 shows how an increase in the pulling velocity affects the adhesive response: the debonding time t_{D} decreases, while the plateau value of $W(t)$, i.e. the adhesion strength G, is enhanced.

The adhesion strength G is plotted against pulling velocity v_{pull} in Fig. 6.19 for different connector lengths and temperatures.

The velocity dependences of the adhesion strength can be fitted as power laws $G \propto v_{\mathrm{pull}}^{\alpha}$, where the exponent α increases with temperature from $\alpha \approx 0.2$ for $T = 0.3$ to $\alpha \approx 1.0$ for $T = 2.0$. As the temperature increases, the system is no longer in the glassy state and the dependence of G on v_{pull} becomes almost linear, as predicted for elastomers (Raphaël and de Gennes 1992).

For a chosen system, the W versus t dependencies at all considered velocities and temperatures can be replotted in normalized units W/G and t/t_{D} as shown in Fig. 6.20. It is interesting to observe that all curves superpose on a unique master curve. This time-temperature superposition is specific for viscoelastic polymers (Ferry 1970, Maugis and Barquins 1978). Consequently, results at various temperatures/pulling velocities can be predicted, without performing the actual experiments, once the master curve is known from previous work.

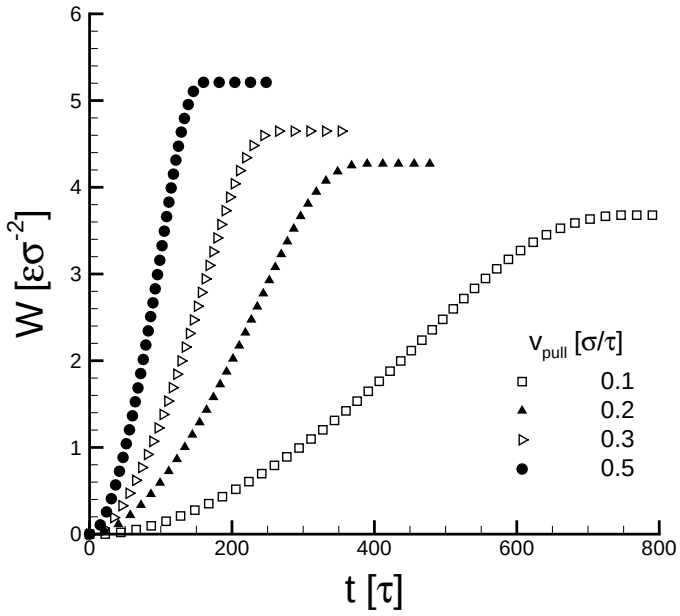

Figure 6.18: *Work of adhesion versus simulation time for different pulling velocities* v_{pull}*. The connectors are symmetric di-block chains with* $n = 100$ *beads per chain.*

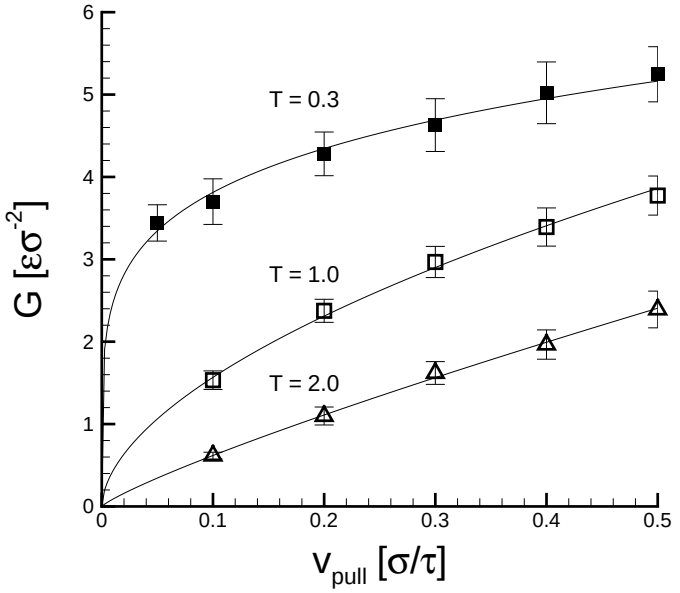

Figure 6.19: *Adhesion strength* G *versus pulling velocity* v_{pull} *for one-stitch connectors with* $n = 100$ *beads at different temperatures. The curves are power fits to the data points.*

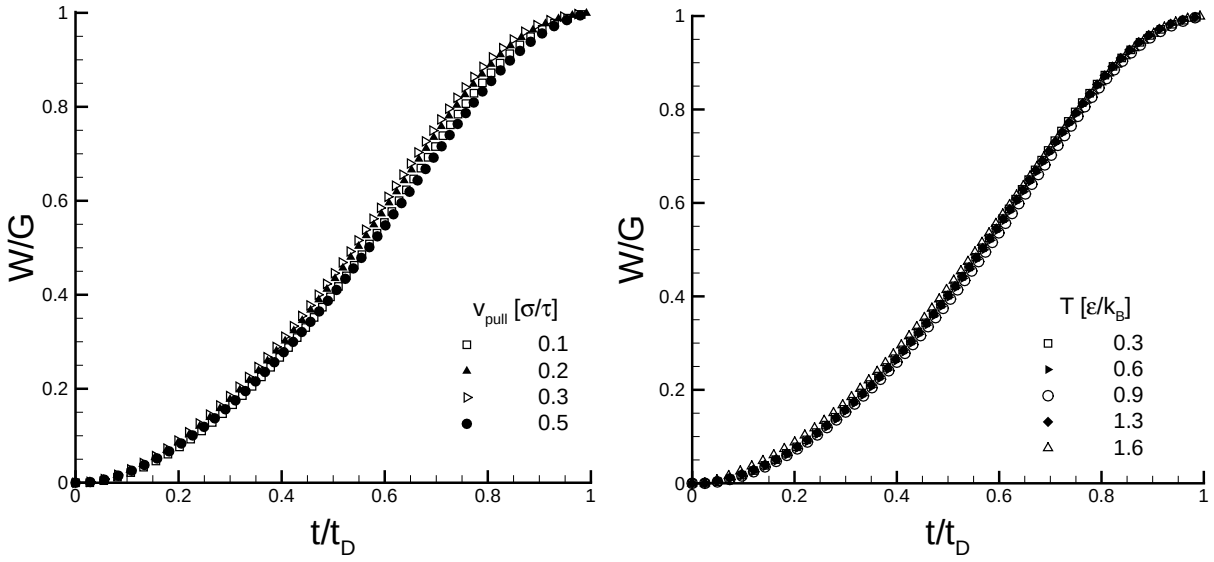

Figure 6.20: *Normalized work W/G versus normalized time t/t_{D} for different pulling velocities at $T = 0.3\varepsilon/k_{\mathrm{B}}$ (left panel) and different temperatures at $v_{\mathrm{pull}} = 0.1\sigma/\tau$ (right panel). All adhesion systems are reinforced with one-stitch symmetric connectors with $n = 100$.*

6.4 Conclusions

In this paper, a detailed molecular dynamics investigation has been performed of an adhesion system formed by placing connector chains at the interface between two glassy polymer bulks. The fracture mechanism considered was chain pullout and we focused on the influence of internal and external parameters on adhesion strength.

The model proposed here is a realistic 3D simulations of tensile debonding of two polymer bulks represented as dense entangled ensembles of linear chains. This gave us the unique possibility to systematically study the influence of the number of stitches formed at the interface on the work of adhesion.

The total work needed to completely pullout the connector chains from the bulks was calculated and comparisons were made between different chain architectures – length and stiffness, number of stitches, areal density – at different pulling velocities and temperatures.

Adhesion strength is mainly influenced by the connector length ($G \propto n^2$) and connector areal density ($G \propto \Sigma$). These scaling laws are unaffected when modifying the connector stiffness or the number of stitches across the interface. A moderate increase in adhesion strength is induced by multiplying the number of stitches or by enhancing connector rigidity.

The results presented here capture also the effect of the pulling velocity, especially

since this was not systematically investigated in previous MD simulations of adhesion. The adhesion strength scales as $v_{\mathrm{pull}}^{\alpha}$ with α dependent on temperature. For low temperatures below T_{g}, $\alpha \approx 0.2$, while for high temperatures, when the system is no longer in the glassy state, the G dependence becomes linear on the pulling velocity, $\alpha \approx 1.0$.

Lowering the temperature of the system induces an increase in adhesion strength. This relationship displays two temperature intervals with different slopes and an apparent glass transition at $T = 1.2\varepsilon/k_{\mathrm{B}}$ is identified. We also found a time-temperature superposition characteristic to viscoelastic polymers: the time evolutions of the adhesion work obtained at various temperatures and pulling velocities superpose on a master curve, when plotted in normalized units.